Understanding Photocatalytic Activity Dependence on Node Topology in Ti-Based Metal–Organic Frameworks

Nikita Kolobov, Abdelali Zaki, Katarzyna Świrk, Partha Maity, Luis Garzon-Tovar, Giasemi Angeli, Alla Dikhtiarenko, Gérard Delahay, Pantelis Trikalitis, Abdul-Hamid Emwas, et al.

Understanding Photocatalytic Activity Dependence on Node Topology in Ti-Based Metal–Organic Frameworks

Nikita Kolobov[1], Abdelali Zaki[2], Katarzyna Świrk[2], Partha Maity[1], Luis Garzon-Tovar[1], Giasemi K. Angeli[3], Alla Dikhtiarenko[4], G. Delahay[2], Pantelis N. Trikalitis[3], Abdul-Hamid Emwas[4], Amandine Cadiau[2], Omar F. Mohammed[5], Christopher H. Hendon[6], Karim Adil[2]*, and Jorge Gascon[1]*

[1] Advanced Catalytic Materials, KAUST Catalysis Center, King Abdullah University of Science and Technology, Thuwal 23955-6900, Saudi Arabia

[2] ICGM, University of Montpellier, CNRS, ENSCM, Montpellier, 34090, France

[3] Department of Chemistry, University of Crete, Heraklion, Crete, 70013, Greece

[4] Imaging and Characterization Department, KAUST Core Laboratories, King Abdullah University of Science and Technology (KAUST), Thuwal 23955, Saudi Arabia;

[5] Advanced Membranes and Porous Materials Center, KAUST Catalysis Center (KCC), Division of Physical Sciences and Engineering, King Abdullah University of Science and Technology (KAUST), Thuwal 23955-6900, Saudi Arabia;

[6] Department of Chemistry and Biochemistry, University of Oregon, Eugene, Oregon 97403, United States

Abstract

Despite the drive to develop more efficient Ti-based metal–organic framework (MOF) photocatalysts, MIL-125-NH2 is still the benchmark, and only a few design principles have been offered to improve photocatalytic performance. Linker functionalization in Ti MOFs has been shown to enable photocatalysis under visible light by closing the electronic band gap, significantly improving charge carrier lifetimes. Limited by known Ti-based MOFs, the role of node nuclearity and topology on photocatalytic activity remains unclear. Here, we report a new MOF, ICGM-1, a 3D-connected framework featuring 1D Ti–O rods. Photocatalytic hydrogen evolution reveals a significant difference in activity, which we attribute solely to node geometry. Using time-resolved spectroscopy and DFT calculations, we ascribe these differences to subtle electronic and geometric properties, paving the way for the development of Ti-MOF photocatalysts.

Introduction

Titanium-based materials have been extensively studied as photocatalysts since the pioneering work from Fujishima and Honda on water splitting using n-type TiO_2. [1] Titanium is not only a highly abundant element, but also displays low toxicity and redox activity (Ti^{III}/Ti^{IV}). In this context, Ti-based MOFs are interesting materials for photocatalysis, since they can integrate light-harvesting properties and catalytic active sites in a single solid. Various Ti-based MOFs have shown promising results in photocatalytic CO_2 reduction, [2] hydrogen evolution, [3–5] and water splitting. [6,7] The versatility in MOF design allows the tuning of light harvesting (band edge positions) and charge separation by the appropriate choice or modification of the building blocks. [8] For instance, the introduction of amino groups to the benzene-dicarboxylate ligand (BDC) in the archetypical MIL-125(Ti) allowed to reduce the optical band gap from ca. 3.7 to 2.6 eV, bringing the photocatalytic response to the visible region. [3,9] In addition, the amino groups are also able to stabilize holes, leading in this way to better charge separation between the photoexcited electron located in the Ti-oxo cluster and the hole located in the amino-terephthalate unit. [10–12] In a similar spirit, the influence of linker expansion for two isoreticular rod-based Ti-MOFs (namely, ZSTU-1 and ZSTU-3) was evaluated. [13] Interestingly, the expansion of the triphenylamine-based ligand in ZSTU-3 results not only in an increase in the optical absorption and lower band gap, but also in a longer lifetime of the photoinduced electron transfer process.

In all these studies, geometry and connectivity of the building blocks and the initial topology of the parent MOFs have not been affected by the modification/expansion of the building units. However, to the best of our knowledge, there are no reports on how the photocatalytic properties of a Ti-based MOF can be affected by changing the geometry of the inorganic building units while maintaining the same organic ligand. Indeed, it is commonly accepted that the discrete nature of the metal-oxo clusters does not allow for high charge mobility because of the absence of orbital overlapping, limiting the MOF photocatalytic activity. [14] In contrast, 1D rods- and chain-based MOFs, such as ZSTU, [13] MIL-177-HT, [15] DIGIST-1, [16] and ACM-1, [5] are expected to present superior photocatalytic performance, as it is hypothesized that infinite Ti-oxo moieties may lead to greater charge mobility, promoting electron/hole separation. [17] Yet, Ti-based MOFs constructed using the

same organic linker but different inorganic building units (discrete oxo-clusters vs rods/chains) have not been reported. This could be attributed to the fact that the synthesis of Ti-based MOFs remains an ongoing challenge due to the complexity of Ti chemistry in solution, in which the fast hydrolysis of the Ti precursors generally causes fast and uncontrollable nucleation, leading mostly to the formation of amorphous phases and/or unpredictable structures. [18]

Herein, we report a new titanium-based MOF, denoted ICGM-1 (Institut Charles Gerhardt Montpellier), based on one-dimensional Ti–O rods and amino-terephthalic acid. As an isomorph to MIL-125-NH2, ICGM-1 is an ideal candidate for a systematic study on the influence of the Ti-node geometry on the photocatalytic properties of the MOFs. Photocatalytic hydrogen evolution reaction (HER) demonstrates a drastic difference in activity solely related to node geometry. Comprehensive characterization together with transient absorption spectroscopy (TAS) and ab initio electronic structure calculations provide evidence that despite the thermodynamic possibility of promoting HER, extended 1D connectivity paired with pore geometry limits HER.

Results

To study the impact of the Ti-SBU geometry on the photocatalytic performance of the Ti-MOFs, we synthesized an isomorph of the photoredox active MIL-125-NH_2 that could be built from the same organic ligand (amino-terephthalic acid) but with a different geometry of the Ti-inorganic building unit. The new Ti-based MOF (ICGM-1) was synthesized by the solvothermal reaction between amino-terephthalic acid, imidazole, and titanium isopropoxide in 2-propanol at 150 °C. Scanning electron microscopy (SEM) analysis performed on the orange polycrystalline material revealed the formation of rod-shaped nanocrystals with crystallite sizes of ~600 nm length and ~100 nm width, which preclude their analysis by single-crystal X-ray diffraction (Figure S1). Consequently, the structure of ICGM-1 was solved using powder X-ray diffraction data (PXRD, Figure S3). The indexation of the ICGM-1 PXRD pattern was performed using the McMaille software, which revealed that ICGM-1 crystallizes in a hexagonal space group P63/mmc (no. 194) with unit cell parameters of a = b = 14.425(4) Å, c = 11.835(7) Å. These cell parameters were confirmed

by the whole powder pattern fit using the Le Bail method with Fullprof software. The extracted diffraction peak intensities were used to solve the structure by direct space methods in a Monte Carlo process with the ESPOIR software, using one TiO_6 octahedron and one amino-terephthalic molecule. The final Rietveld refinement led to satisfactory results (Table S1, Supporting Information) and allowed the determination of the chemical formula as $Ti_6O_9(C_8H_5NO_4)_3$.

In ICGM-1, each Ti^{4+} is surrounded by four μ-O (3 μ3 and 1 μ2) and two oxygen atoms belonging to two crystallographically related amino-terephthalate ligands, giving rise to infinite rods that can be described alternatively as the vertex sharing of hexanuclear clusters ($Ti_6O_{12}(CO_2)_6$). This 1D Ti–O rod SBU was also observed for ZSTU-1–3 and MIL-177 and is in contrast to the cyclic octamers $Ti_8O_8(OH)_4(CO_2)_{12}$ (Figure 1, bottom) observed in MIL-125-NH_2. [13] Each hexagonal $Ti_6O_9(CO_2)_6$ subunit of the infinite rod is connected to six amino-terephthalate linkers to generate a 3-periodic MOF (Figure 1, top) with the underlying hxl topology.

ICGM-1 presents channels along the c-axis where the aperture size calculated from the distance of opposite hydrogen atoms (excluding the Van Der Waals radius) is 3.0 Å. Given that the kinetic diameter of N_2 is 3.64 Å, a very limited adsorption is expected even at its boiling point (77 K), and this is confirmed experimentally (Figure S4). To probe the pore structure of ICGM-1 and investigate its sorption properties, we recorded H_2O (kinetic diameter, 2.65 Å) isotherms at 298 K. Accordingly, the H_2O uptake and saturation pressure (p/p_0 = 1, or RH = 100%) is 200.2 cm^3(STP) g^{-1} (8.9 mmol g^{-1}; Figure S5). Considering the liquid density of H_2O at 298 K (0.997 cm^3 g^{-1}), the calculated total pore volume at 0.99p/p_0 is 0.16 cm^3 g^{-1}, which is very close to the value obtained from the single-crystal structure, indicating that the pore system in ICGM-1 is fully accessible. With this pore size, ICGM-1 has no issue with HER half-reaction since H_2O plays the role of the proton source, however, oxidation part of the photocatalytic process could be substantially limited. The chemical stability of ICGM-1 was confirmed by PXRD analysis after treatment of the powder at different pH (3–10) for 24 h, revealing that the crystal structure remains unaffected (Figure S7). The thermal stability of ICGM-1 was evaluated by TGA (Figure S8) and variable-

temperature powder X-ray diffraction (VT-PXRD, Figure S9) performed in the range of 25–400 °C, establishing that the material retained its crystallinity up to 300 °C.

Finally, MIL-125-NH_2 was synthesized following the reported methodology. [19] The phase purity was confirmed by PXRD (Figure S10) together with N_2 adsorption (Figure S11).

Diffuse reflectance UV–vis spectroscopy of both MIL-125-NH_2 and ICGM-1 shows small differences in light absorption. ICGM-1 showed a red shift to ~600 nm when compared to MIL-125-NH_2 (~500 nm; Figure 2a). In addition, the maximum absorption of ICGM-1 is at 410 nm in contrast to the observed for MIL-125-NH_2 (380 nm). This absorption can be assigned to the LMCT process and the light-induced electron transfer from NH_2-bdc to the vacant Ti^{4+} d-orbitals, resulting in Ti^{IV} to Ti^{III} reduction. [12,20] The formation of Ti^{III} upon illumination (and therefore successful ligand to metal charge transfer) was confirmed in both cases by electron paramagnetic resonance (EPR) spectroscopy [2,3,21,22] after visible-light irradiation in acetonitrile in the presence of triethylamine (TEA) as a sacrificial agent (Figure S13).

The optical band gap energies derived from the respective Tauc plots [23] (Figure S14) were estimated to be 2.8 and 2.6 eV for MIL-125-NH_2 and ICGM-1, respectively. These results, in combination with photoelectron spectroscopy in air (PESA), led to the calculation of the band alignments presented in Figure 2b. In both cases, the MOFs span the redox potential of H_2O. Similarly, both ICGM-1 and MIL-125-NH_2 share a similar HOCO (highest occupied crystal orbital) level (around −5.8 eV) derived from the NH_2-bdc, while the LUCO (lowest unoccupied crystal orbital) level of ICGM-1 resulted to be lower by ~0.2 eV.

The photocatalytic activity of the two MOFs was evaluated for HER in the absence and presence of photodeposited Pt as cocatalyst. [24] We used a Xe lamp coupled with a cutoff filter ($\lambda > 380$ nm) for irradiation of the MOF suspension in ACN/H_2O/TEA mixture with a density of 1 mg/mL. Triethylamine has been used as a sacrificial agent. Figure 2c shows the obtained HER reaction rates for MIL-125-NH_2 and ICGM-1 with and without the photodeposited Pt. In the presence of Pt, MIL-125-NH_2 displays a significantly higher

activity, ca. 6 times that of ICGM-1. Surprisingly, in the absence of Pt, no hydrogen evolution was observed when ICGM-1 was used, in sharp contrast to MIL-125-NH_2. Both MOFs poses moderate photocatalytic stability (Figure S15).

To demonstrate that the difference in the photocatalytic performance was not derived solely from differences in surface areas, we also synthesized the isoreticular version of ICGM-1 using NH_2-bpdc (2-amino-1,1′-biphenyl-4,4′-dicarboxylate) (Figure S16). The photocatalytic results demonstrate even lower activity in HER. Finally, we confirmed by PXRD analysis that the structure of both ICGM-1 and MIL-125-NH_2 remain unaltered after the photocatalytic measurements, confirming the high stability of the materials (Figure S17).

One of the possible reasons for the absence of activity for the bare ICGM-1 could be a higher probability of stabilized e−−H+ pairs on bridging oxygen atoms in comparison to MIL-125-NH_2. Recently, Mancuso et al. [25] demonstrated by computational and experimental means that proton-stabilized reduced MIL-125 is more stable than HER in the low-charging regime. At the same time, the drastic difference in activity in the presence of a cocatalyst could be related to the charge-carriers dynamics and excited states lifetime. [20]

To understand the origin of ICGM-1's HER performance, we performed electronic structure calculations on both MIL-125-NH_2 and ICGM-1 using density functional theory (DFT). First, we performed geometry optimization on primitive cells using PBEsol functional as a cost-effective and reliable approach. Finally, we used HSE06sol functional to recover a reliable band gap value. [26,27] The ionization potential was then computed by vacuum level alignment. [28] The computational ionization potentials were found to be in excellent agreement with those presented in Figure 2b. Density of states (DOS) presented in Figure 3 show that both MOFs feature CBMs composed of O 2p and Ti 3d orbitals, [29] positioned higher than the reduction potential of $2H^+/H_2$ (−4.44 eV, pH = 0). Thus, both materials have appropriate thermodynamic alignment for HER. VBMs are represented by 2p orbitals of C and N from the bdc-NH_2 linker. Interestingly, the estimated bandgap value of ICGM-1 is 2.54 eV, which is 60 meV smaller in comparison to MIL-125-NH_2 (2.6 eV) and follows the same trend as in the UV−vis results.

As discussed above, the formation of stabilized $Ti^{III}–OH^{+}$ pairs previously reported [25] might be behind the poor catalytic performance of the ICGM material. The apparent bandgap reduction (the reversible colorless-to-black transformation, Ti^{III}-formation) of MIL-1253 and recent experimental results for charge accumulation on the Ti_8 nodes [30] suggest that a significant portion of photogenerated $Ti^{III}–OH^{+}$ remain stable toward HER, thus suppressing H_2 formation. Hendon and co-workers demonstrated that, in the case of MIL-125, a single $H^{\bullet}$ added to a μ2-O in the $Ti_8O_8(OH)_4(CO_2)_{12}$ node leads to the formation of a "mid-gap" state (Ti-centered) lying 100 meV below the H^{+}/H_2 reduction potential. [25]

We performed similar calculations to study the possibility of the formation of stable $Ti^{III}–OH^{+}$ species in MIL-125-NH_2 and ICGM-1, respectively. First, we sampled a single $H^{\bullet}$ added to a bridging μ2-oxo of MIL-125-NH_2. The results show the stabilization of a Ti-centered orbital at −4.25 eV (slightly above the HER potential, Figure 4, first column). Examination of $2H^{*}$ on geminal μ2-oxo yielded HER-stable Ti^{III} species (−4.60 eV, Figure 4, second column).

The case of ICGM-1 is slightly more complex, since the $H^{\bullet}$ can, in principle, be allocated in two different positions: the μ3-oxo of $Ti_6O_9(CO_2)_6$ cluster-subunit (H_n, Figure 4, third column) or the μ2-oxo between two $Ti_6O_9(CO_2)_6$ subunits (Hb, Figure 4, fourth column) in the rod. Both are energetically similar. Hb is energetically disfavored by ~5.4 kcal/mol; however, both Hn and Hb are unstable toward HER (above HER potential). The addition of one extra $H^{\bullet}$ leads to three possible configurations, 2Hnn, 2Hbb, and 2Hnb, with similar formation energies (depicted on Figure 4, fifth, sixth, and seventh columns, respectively). Surprisingly, all three configurations remain unstable toward HER and thus do not crate any restrictions to the photocatalytic process. Moreover, the total energy difference between pristine materials and $H^{\bullet}$ and $2H^{\bullet}$ configurations (Table S2) indicates that the formation of $Ti^{III}–OH^{+}$ is more favorable for ICGM-1. Thus, results of DFT calculations for both MOFs suggest the accumulation of e^{-}/H^{+} pairs and less probable H_2 generation for MIL-125-NH_2 rather than for ICGM-1 and contradict the experimental observation.

Along with the energetic requirements of visible-light absorbance and band-edge alignment for desired redox processes, the kinetics of photoexcited states (charge carriers dynamics) directly correlate with photocatalytic performance. [17] Thus, the lifetime of the photogenerated charge carriers (electrons and holes) has to be sufficiently long for the redox reactions to compete with the recombination process. Time-resolved spectroscopy is a powerful tool to study light-induced charge carrier dynamics in a wide range of time scales (from femto- to microsecond). [31] Thus, to evaluate the charge recombination properties of our materials, we performed transient absorption (TA) spectroscopy.

The TA spectra at different delay times for MIL-125-NH_2 and ICGM-1 suspensions in acetonitrile upon 350 nm optical excitation are presented in Figure 5a and b, respectively. The TA spectra of both MIL-125-NH_2 and ICGM-1 are mainly dominated by the photobleach (PB) signal due to the depletion of the ground state of the system, which agrees well with the steady-state absorption spectra presented in Figure S18. To get insight into the charge recombination dynamics and validates the HER, we compared the normalized PB recovery kinetics at 440 nm for both MIL-125-NH_2 and ICGM-1, as displayed in Figure 5c. As can be seen in the Figure 5c, the charge recombination rate is significantly slower for MIL-125-NH_2 ($\tau1$ = 0.70 µs, 95%; $\tau2$ = 2.8 µs, 5%) than for ICGM-1 ($\tau1$ = 0.02 µs, 86%; $\tau2$ = 0.38 µs, 14%), indicating the longer-lived photogenerated charge carriers in the case of MIL-125-NH2. Thus, the information extracted from the TA analysis allows to conclude that MIL-125-NH_2 is expected to be a more efficient photocatalyst. In other words, the shorter lifetime of the excited states of ICGM-1 may not allow the efficient utilization of the photogenerated charge carriers.

MOFs being known as poor photoconductors due to their porous nature and lack of conjugation, usually display a “hopping” transport mechanism. [32] According to the band transport model, mobility of charge carriers in a given material is related to its effective mass m*. As a result mobility could be estimated based on the degree of dispersion of CBM and VBM. [33] For example, it has been demonstrated that for the Ti-chain based MOF ACM, the effective mass of the excited electron is lowest in the Ti–O–Ti–O chains direction, whereas the hole on the pyrene linker is an order of magnitude heavier. [5]

Thus, we evaluated the electron and hole mobilities for MIL-125-NH_2 and ICGM-1 by calculating charge carrier's effective masses based on band transport model. [33] The m* is inversely proportional to the charge mobility, thus large/small values of m* correspond to low/high photoconductivity. Considering that PBEsol and HSE06sol functionals yield to a similar band dispersion at VBM and CBM, and the only difference is the bandgap value, more cost-effective PBEsol has been chosen for the effective mass calculations. The computed m* along different k-point paths are represented in Table 1, where m_0 is electron rest mass.

The VBM are represented by flat bands and nearly infinite m* hole mass in both cases due to highly localized nature of NH_2 groups. In the case of CBM, the presence of NH2 groups does not alternate the dispersion of CBM (Ti 3d formed), but inherently lowers the symmetry of the structure, formally, to P1. The result is that bands are artificially split because of the system desymmetrization (Figure S19). Nevertheless, we can still compute the band structure as if it adheres to the parent material, rather than a P1 system (since P_1 has no high symmetry points). Analysis of the band dispersion reveals, that MIL-125-NH_2 demonstrates lower electron effective mass ($0.67m_0$) along Γ → Z path, which corresponds to the vector perpendicular to octameric titanium wheels in real space. Meanwhile, the lowest electron effective mass for ICGM-1 displayed at Γ → K path ($0.91m_0$, perpendicular to the ROD in real space) and effective mass at Γ → A (along the ROD in real space) path is >50m0.

These results contradict the statement that 1D Ti–O rods [13] might be better than Ti-MOFs with discrete Ti–O clusters. The reason for the reduced band dispersion in the 1D chain is that the Ti–O rod has linear μ2-oxo and μ3-oxo, and they are very different in energy. An analysis of the electron density of lowest unoccupied crystal orbital (LUCO) of ICGM-1 (no NH2) and MIL-125 allows us to demonstrate this difference. Figure 5d shows the electron density of the first unoccupied band in the ICGM-1 (no NH_2) and MIL-125, it is clearly seen that the $Ti_6O_9(CO_2)_6$ clusters are electronically isolated in the 1D channel, meanwhile, the

electronic density in octameric $Ti_8O_8(OH)_4(CO_2)_{12}$ is more evenly distributed between Ti 3d and O 2p orbitals of μ2-oxo species. Additionally, substantial charge distribution locates on the C atoms in case of MIL-125. We believe that it is related to the level of hybridization of the CBM and the stronger bonding between Ti, O, and C atoms, which enables a higher degree of band dispersion (17) (charge mobility) in the CBM of MIL-125.

In this work, we have introduced ICGM-1, a new Ti-based MOF, as tool to better understand photocatalytic behavior of Ti-based MOFs. When compared to the archetypical MIL-125 (Ti), both structures, having the same metal and linker, show a significant difference in their ability to produce H_2, emphasizing the importance of node topology. DFT calculations have shown the absence of potential barriers derived from the formation of stable $Ti^{III}–OH^+$ species in ICGM-1. Band structure calculations revealed drastic differences in effective masses of electrons and holes for these two materials, electrons of MIL-125-NH_2 have lower effective mass than ICGM-1 and, as a result, higher mobility. The latter has been further confirmed by transient absorption spectroscopy, where a longer lifetime for photogenerated charge carriers in case of MIL-125-NH_2 was evident. Our study presents evidence that challenges the recent speculation that Ti-MOFs with Ti–O rods are inherently more efficient photocatalysts than Ti-MOFs with discrete metal oxide clusters. We believe this study may contribute to a better understanding of photocatalysis in Ti MOFs and should enable the design of more efficient materials.

Funding

Funding for this work was provided by King Abdullah University of Science and Technology (KAUST).

Notes

The authors declare no competing financial interest.

Acknowledgments

Funding for this work was provided by King Abdullah University of Science and Technology (KAUST) This work is based upon work supported by the National Science Foundation through the Division of Materials Research under Grant No. DMR-1956403. C.H.H. also acknowledges the Camille and Henry Dreyfus Foundation.

References

1 Fujishima, A.; Honda, K. Electrochemical Photolysis of Water at a Semiconductor Electrode. Nature 1972, 238, 37– 38, DOI: 10.1038/238037a0

2 Fu, Y.; Sun, D.; Chen, Y.; Huang, R.; Ding, Z.; Fu, X.; Li, Z. An Amine-Functionalized Titanium Metal-Organic Framework Photocatalyst with Visible-Light-Induced Activity for CO_2 Reduction. Angew. Chem., Int. Ed. 2012, 51, 3364– 3367, DOI: 10.1002/anie.201108357

3 Horiuchi, Y.; Toyao, T.; Saito, M.; Mochizuki, K.; Iwata, M.; Higashimura, H.; Anpo, M.; Matsuoka, M. Visible-Light-Promoted Photocatalytic Hydrogen Production by Using an Amino-Functionalized Ti(IV) Metal-Organic Framework. J. Phys. Chem. C 2012, 116, 20848– 20853, DOI: 10.1021/jp3046005

4 Castells-Gil, J.; M. Padial, N.; Almora-Barrios, N.; da Silva, I.; Mateo, D.; Albero, J.; García, H.; Martí-Gastaldo, C. De novo synthesis of mesoporous photoactive titanium(iv)-organic frameworks with MIL-100 topology. Chem. Sci. 2019, 10, 4313– 4321, DOI: 10.1039/C8SC05218B [

5 Cadiau, A.; Kolobov, N.; Srinivasan, S.; Goesten, M. G.; Haspel, H.; Bavykina, A. V.; Tchalala, M. R.; Maity, P.; Goryachev, A.; Poryvaev, A. S. A Titanium Metal-Organic Framework with Visible-Light-Responsive Photocatalytic Activity. Angew. Chem., Int. Ed. 2020, 59, 13468– 13472, DOI: 10.1002/anie.202000158

6 Remiro-Buenamañana, S.; Cabrero-Antonino, M.; Martínez-Guanter, M.; Álvaro, M.; Navalón, S.; García, H. Influence of co-catalysts on the photocatalytic activity of MIL-125(Ti)-NH2 in the overall water splitting. Appl. Catal., B 2019, 254, 677– 684, DOI: 10.1016/j.apcatb.2019.05.027

7 Salcedo-Abraira, P.; Babaryk, A. A.; Montero-Lanzuela, E.; Contreras-Almengor, O. R.; Cabrero-Antonino, M.; Grape, E. S.; Willhammar, T.; Navalón, S.; Elkäim, E.; García, H. A Novel Porous Ti-Squarate as Efficient Photocatalyst in the Overall Water Splitting Reaction under Simulated Sunlight Irradiation. Adv. Mater. 2021, 33, 2106627, DOI: 10.1002/adma.202106627

8 Kolobov, N.; Goesten, M. G.; Gascon, J. Metal-Organic Frameworks: Molecules or Semiconductors in Photocatalysis?. Angew. Chem., Int. Ed. 2021, 60, 26038– 26052, DOI: 10.1002/anie.202106342

9 Hendon, C. H.; Tiana, D.; Fontecave, M.; Sanchez, C.; D'arras, L.; Sassoye, C.; Rozes, L.; Mellot-Draznieks, C.; Walsh, A. Engineering the Optical Response of the Titanium-MIL-125 Metal-Organic Framework through Ligand Functionalization. J. Am. Chem. Soc. 2013, 135, 10942– 10945, DOI: 10.1021/ja405350u

10 Santaclara, J. G.; Nasalevich, M. A.; Castellanos, S.; Evers, W. H.; Spoor, F. C. M.; Rock, K.; Siebbeles, L. D. A.; Kapteijn, F.; Grozema, F.; Houtepen, A. Organic Linker Defines the Excited-State Decay of Photocatalytic MIL-125(Ti)-Type Materials. ChemSusChem 2016, 9, 388– 395, DOI: 10.1002/cssc.201501353

11 Capano, G.; Ambrosio, F.; Kampouri, S.; Stylianou, K. C.; Pasquarello, A.; Smit, B. On the Electronic and Optical Properties of Metal-Organic Frameworks: Case Study of MIL-125 and MIL-125-NH2. J. Phys. Chem. C 2020, 124, 4065– 4072, DOI: 10.1021/acs.jpcc.9b09453 [

12 de Miguel, M.; Ragon, F.; Devic, T.; Serre, C.; Horcajada, P.; García, H. Evidence of Photoinduced Charge Separation in the Metal-Organic Framework MIL-125(Ti)-NH_2. ChemPhysChem 2012, 13, 3651– 3654, DOI: 10.1002/cphc.201200411

13 Li, C.; Xu, H.; Gao, J.; Du, W.; Shangguan, L.; Zhang, X.; Lin, R.-B.; Wu, H.; Zhou, W.; Liu, X. Tunable titanium metal-organic frameworks with infinite 1D Ti-O rods for efficient visible-light-driven photocatalytic H_2 evolution. J. Mater. Chem. A 2019, 7, 11928– 11933, DOI: 10.1039/C9TA01942A

14 Yan, Y.; Li, C.; Wu, Y.; Gao, J.; Zhang, Q. From isolated Ti-oxo clusters to infinite Ti-oxo chains and sheets: recent advances in photoactive Ti-based MOFs. J. Mater. Chem. A 2020, 8, 15245– 15270, DOI: 10.1039/D0TA03749D

15 Wang, S.; Kitao, T.; Guillou, N.; Wahiduzzaman, M.; Martineau-Corcos, C.; Nouar, F.; Tissot, A.; Binet, L.; Ramsahye, N.; Devautour-Vinot, S. A phase transformable ultrastable titanium-carboxylate framework for photoconduction. Nat. Commun. 2018, 9, 1660, DOI: 10.1038/s41467-018-04034-w

16 Keum, Y.; Park, S.; Chen, Y.-P.; Park, J. Titanium-Carboxylate Metal-Organic Framework Based on an Unprecedented Ti-Oxo Chain Cluster. Angew. Chem., Int. Ed. 2018, 57, 14852– 14856, DOI: 10.1002/anie.201809762

17 Fumanal, M.; Ortega-Guerrero, A.; Jablonka, K. M.; Smit, B.; Tavernelli, I. Charge Separation and Charge Carrier Mobility in Photocatalytic Metal-Organic Frameworks. Adv. Funct. Mater. 2020, 30, 2003792, DOI: 10.1002/adfm.202003792

18 Assi, H.; Mouchaham, G.; Steunou, N.; Devic, T.; Serre, C. Titanium coordination compounds: from discrete metal complexes to metal-organic frameworks. Chem. Soc. Rev. 2017, 46, 3431– 3452, DOI: 10.1039/C7CS00001D

19 Santaclara, J. G.; Olivos-Suarez, A. I.; du Fossé, I.; Houtepen, A.; Hunger, J.; Kapteijn, F.; Gascon, J.; van der Veen, M. A. Harvesting the photoexcited holes on a photocatalytic proton reduction metal-organic framework. Faraday Discuss. 2017, 201, 71– 86, DOI: 10.1039/C7FD00029D

20 Nasalevich, M. A.; Hendon, C. H.; Santaclara, J. G.; Svane, K.; van der Linden, B.; Veber, S. L.; Fedin, M. V.; Houtepen, A. J.; van der Veen, M. A.; Kapteijn, F. Electronic origins of photocatalytic activity in d0 metal organic frameworks. Sci. Rep. 2016, 6, 23676, DOI: 10.1038/srep23676

21 Dan-Hardi, M.; Serre, C.; Frot, T.; Rozes, L.; Maurin, G.; Sanchez, C.; Férey, G. A New Photoactive Crystalline Highly Porous Titanium(IV) Dicarboxylate. J. Am. Chem. Soc. 2009, 131, 10857– 10859, DOI: 10.1021/ja903726m

22 Castells-Gil, J.; Padial, N. M.; Almora-Barrios, N.; Albero, J.; Ruiz-Salvador, A. R.; González-Platas, J.; García, H.; Martí-Gastaldo, C. Chemical Engineering of Photoactivity in Heterometallic Titanium-Organic Frameworks by Metal Doping. Angew. Chem., Int. Ed. 2018, 57, 8453– 8457, DOI: 10.1002/anie.201802089

23 Makuła, P.; Pacia, M.; Macyk, W. How To Correctly Determine the Band Gap Energy of Modified Semiconductor Photocatalysts Based on UV-Vis Spectra. J. Phys. Chem. Lett. 2018, 9, 6814– 6817, DOI: 10.1021/acs.jpclett.8b02892

24 Gong, Y.-N.; Mei, J.-H.; Liu, J.-W.; Huang, H.-H.; Zhang, J.-H.; Li, X.; Zhong, D.-C.; Lu, T.-B. Manipulating metal oxidation state over ultrastable metal-organic frameworks for boosting photocatalysis. Appl. Catal., B 2021, 292, 120156, DOI: 10.1016/j.apcatb.2021.120156

25 Mancuso, J. L.; Fabrizio, K.; Brozek, C. K.; Hendon, C. H. On the limit of proton-coupled electronic doping in a Ti(iv)-containing MOF. Chem. Sci. 2021, 12, 11779– 11785, DOI: 10.1039/D1SC03019A

26 Mancuso, J. L.; Mroz, A. M.; Le, K. N.; Hendon, C. H. Electronic Structure Modeling of Metal-Organic Frameworks. Chem. Rev. 2020, 120, 8641– 8715, DOI: 10.1021/acs.chemrev.0c00148

27 Fabrizio, K.; Le, K. N.; Andreeva, A. B.; Hendon, C. H.; Brozek, C. K. Determining Optical Band Gaps of MOFs. ACS Mater. Lett. 2022, 4, 457– 463, DOI: 10.1021/acsmaterialslett.1c00836 [ACS

28 Butler, K. T.; Hendon, C. H.; Walsh, A. Electronic Chemical Potentials of Porous Metal-Organic Frameworks. J. Am. Chem. Soc. 2014, 136, 2703– 2706, DOI: 10.1021/ja4110073

29 Mancuso, J. L.; Hendon, C. H. Titanium(IV) Inclusion as a Versatile Route to Photoactivity in Metal-Organic Frameworks. Adv. Theory Simul. 2019, 2, 1900126, DOI: 10.1002/adts.201900126

30 Saouma, C. T.; Richard, S.; Smolders, S.; Delley, M. F.; Ameloot, R.; Vermoortele, F.; De Vos, D. E.; Mayer, J. M. Bulk-to-Surface Proton-Coupled Electron Transfer Reactivity of the Metal-Organic Framework MIL-125. J. Am. Chem. Soc. 2018, 140, 16184– 16189, DOI: 10.1021/jacs.8b09120

31 Pattengale, B.; Ostresh, S.; Schmuttenmaer, C. A.; Neu, J. Interrogating Light-initiated Dynamics in Metal-Organic Frameworks with Time-Resolved Spectroscopy. Chem. Rev. 2022, 122, 132, DOI: 10.1021/acs.chemrev.1c00528

32 Xie, L. S.; Skorupskii, G.; Dincă, M. Electrically Conductive Metal-Organic Frameworks. Chem. Rev. 2020, 120, 8536– 8580, DOI: 10.1021/acs.chemrev.9b00766

33 Oberhofer, H.; Reuter, K.; Blumberger, J. Charge Transport in Molecular Materials: An Assessment of Computational Methods. Chem. Rev. 2017, 117, 10319– 10357, DOI: 10.1021/acs.chemrev.7b00086

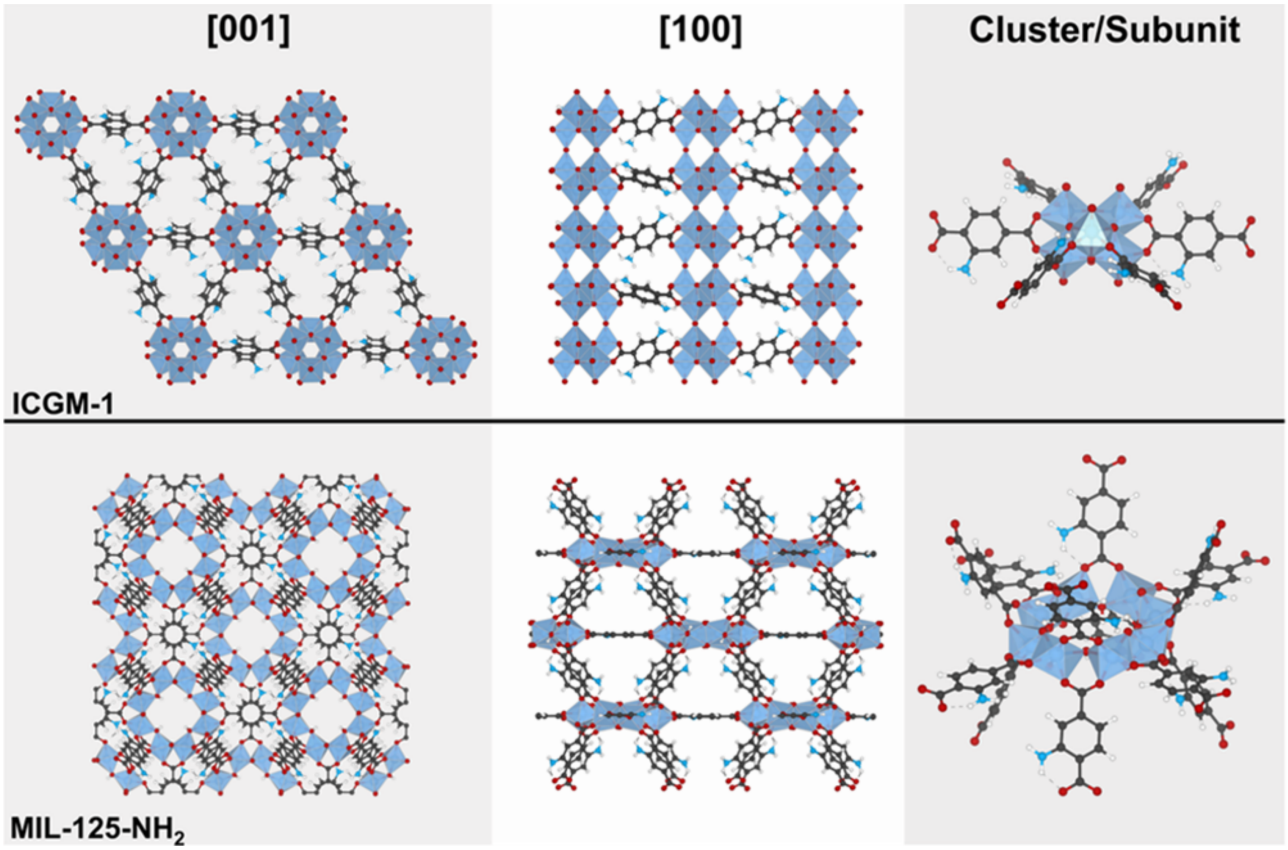

Figure 1. (Top) ICGM-1 structure view along [001] and [100] directions; $Ti_6O_9(CO_2)_6$ (ICGM-1) cluster-subunit (bottom) MIL-125-NH_2 structure view along [001] and [100] directions; $Ti_8O_8(OH)_4(CO_2)_{12}$ (MIL-125-NH_2) cluster-subunit.

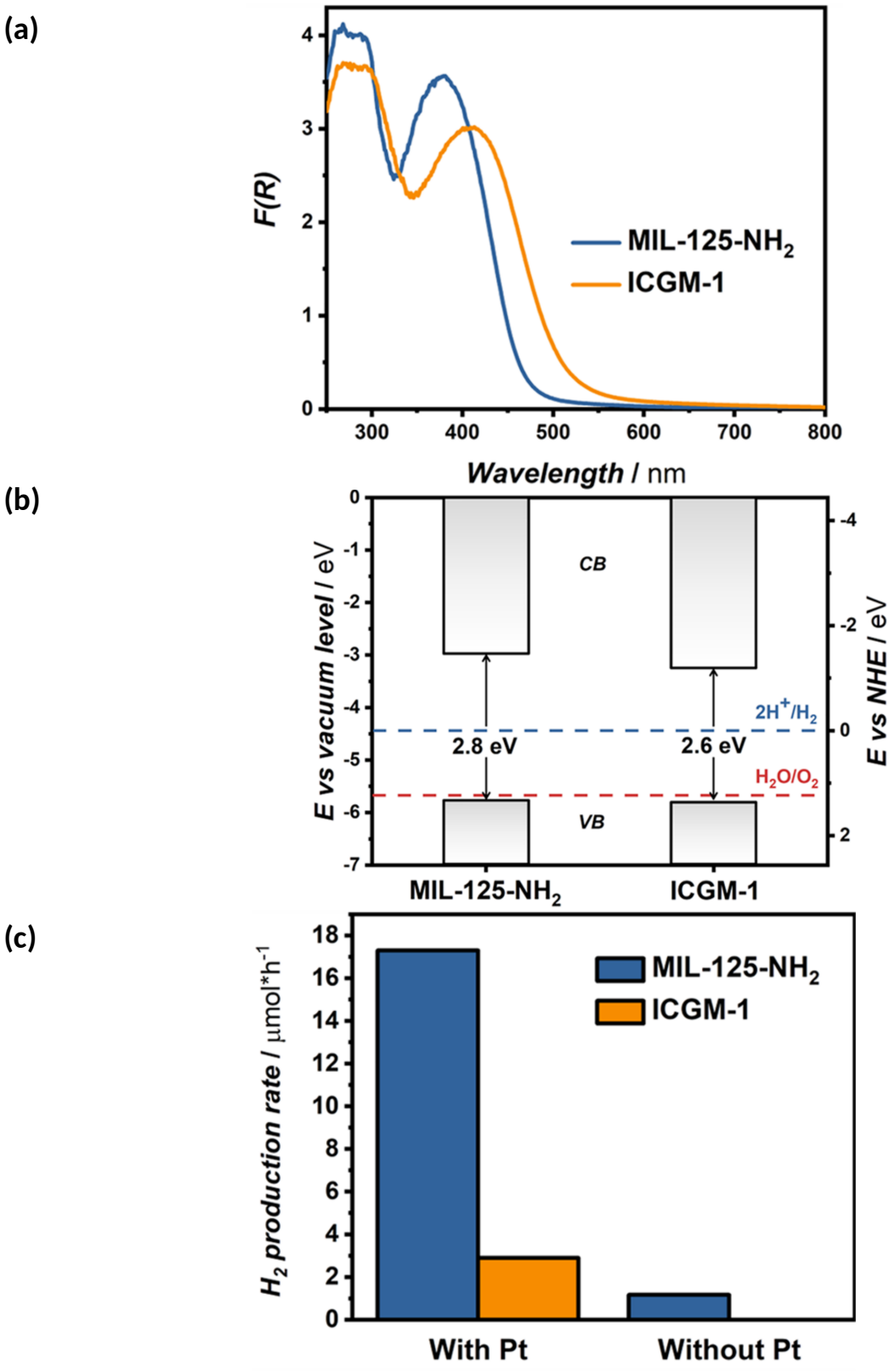

Figure 2. (a) Diffuse reflectance UV–vis spectra of the ICGM-1 and MIL-125-NH_2. (b) Band alignment of ICGM-1 and MIL-125-NH_2 vs vacuum. (c) ICGM-1 and MIL-125-NH_2 photocatalytic activity in HER.

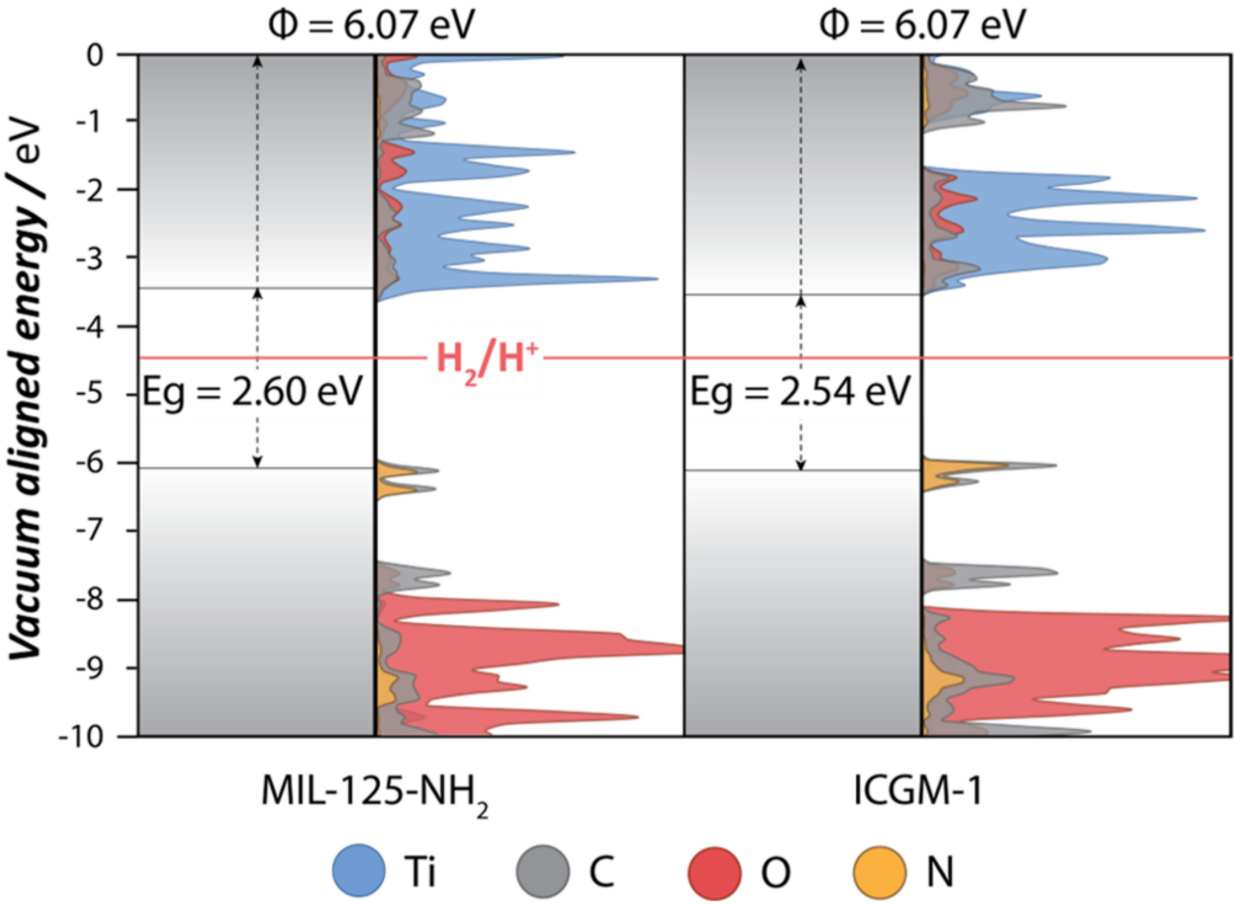

Figure 3. Vacuum-aligned DOS plots show that both MIL-125-NH_2 and ICGM-1 have CBMs above H^+/H_2 (−4.44 eV, shown in red).

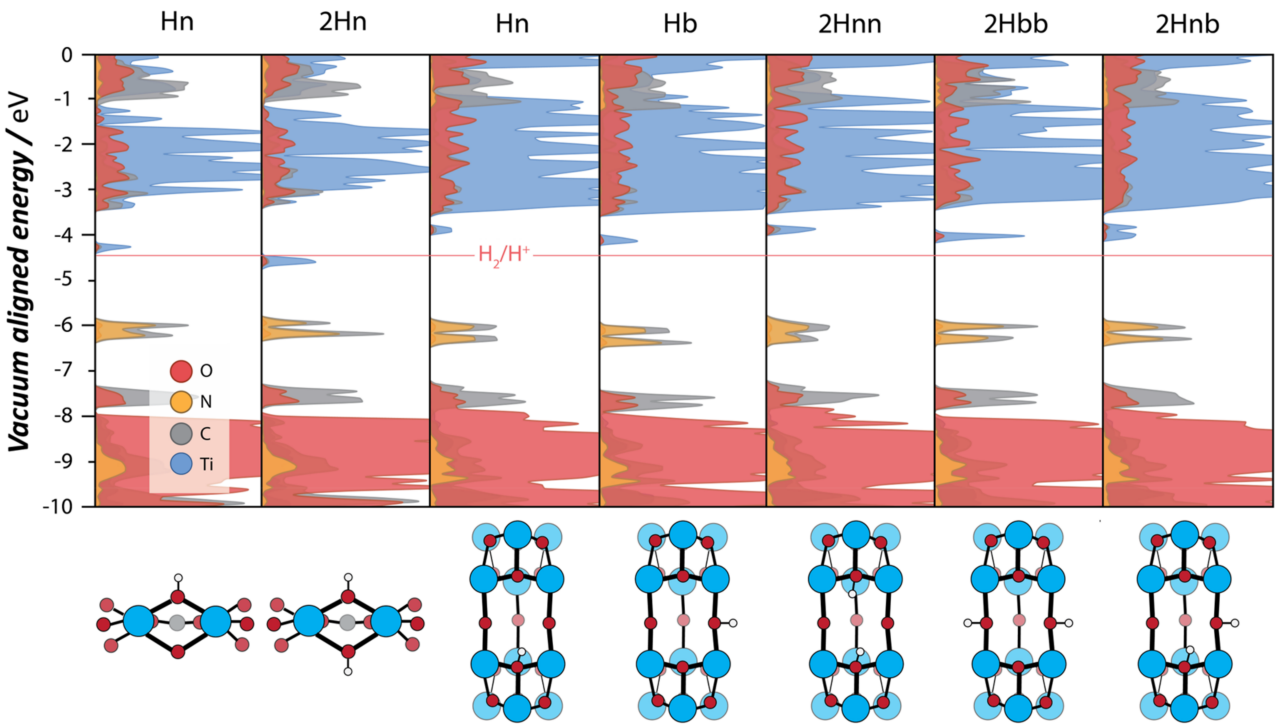

Figure 4. (Top) The vacuum-aligned atom-projected DOS plots for different Ti^{III}–OH^{+} configurations. (Bottom) A schematic depiction of added H* to the μ2-oxos of MIL-125-NH_2 and ICGM-1.

(a)

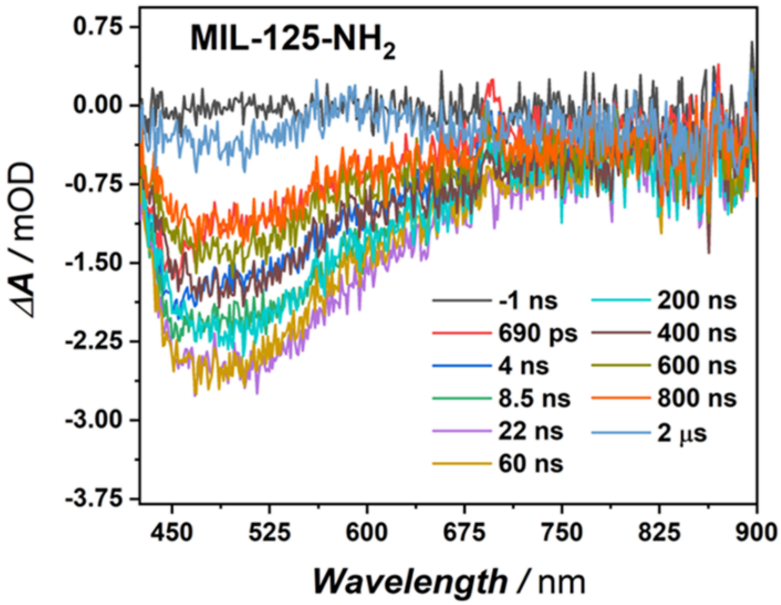
MIL-125-NH2
ΔA / mOD
Wavelength / nm
-1 ns
690 ps
4 ns
8.5 ns
22 ns
60 ns
200 ns
400 ns
600 ns
800 ns
2 μs

(b)

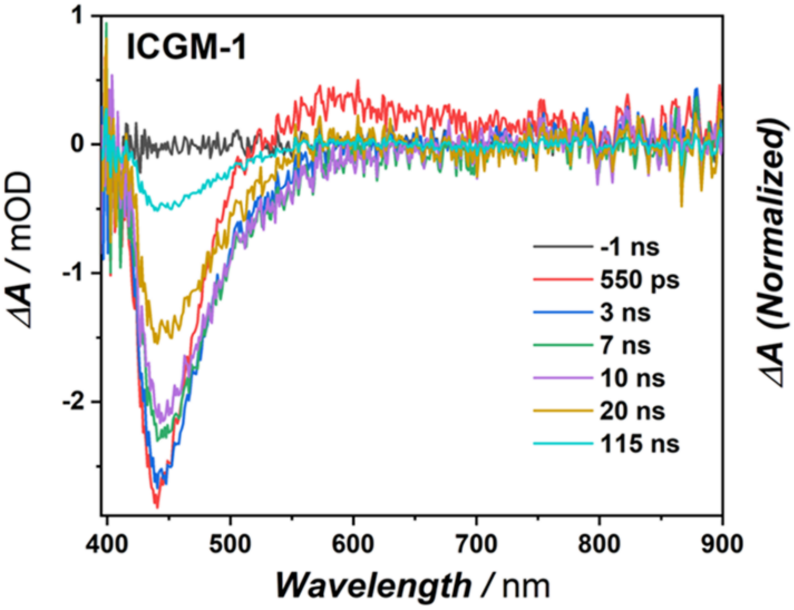
ICGM-1
ΔA / mOD
ΔA (Normalized)
Wavelength / nm
-1 ns
550 ps
3 ns
7 ns
10 ns
20 ns
115 ns

(c)

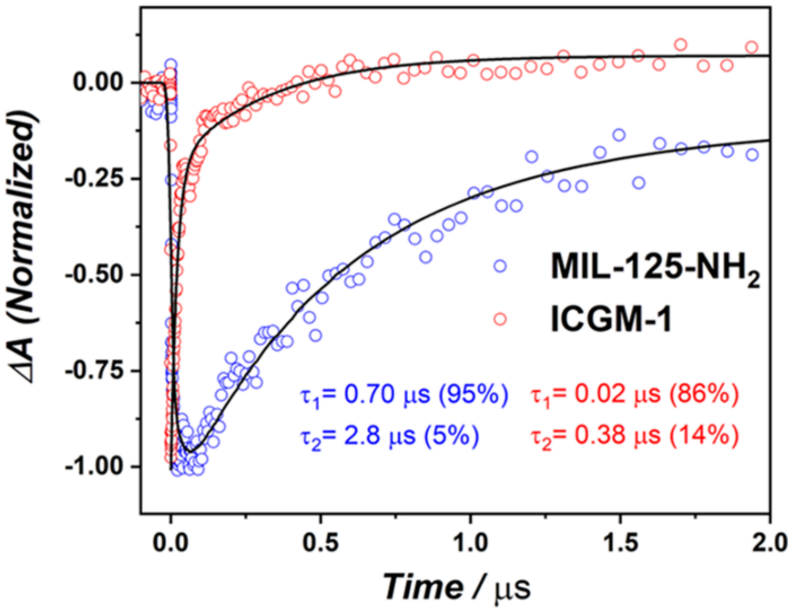
ΔA (Normalized)
Time / μs
MIL-125-NH2
ICGM-1
τ1= 0.70 μs (95%)
τ2= 2.8 μs (5%)
τ1= 0.02 μs (86%)
τ2= 0.38 μs (14%)

(d)

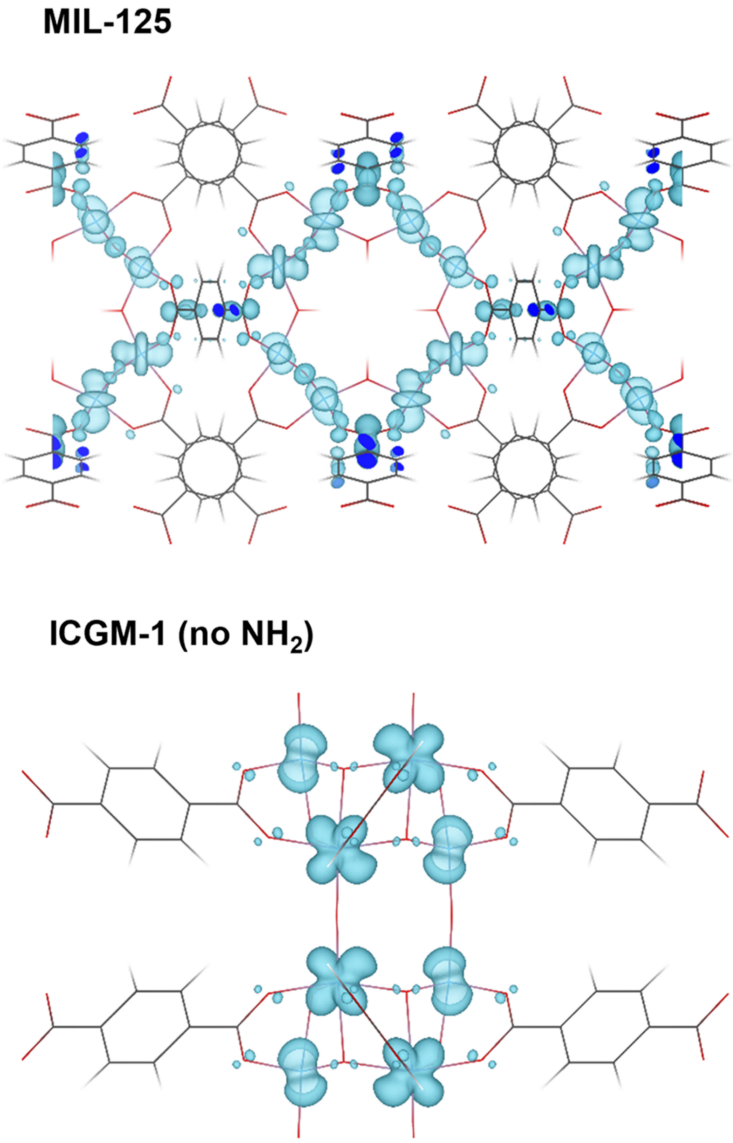

Figure 5. Transient absorption spectra at various delay time of (a) MIL-125-NH_2 and (b) ICGM-1 in ACN solution in response to 350 nm optical excitation; (c) Normalized PB recovery kinetics probed at 440 nm of ICGM-1 and MIL-125-NH_2 in ACN; (d) Isodensity representation of the LUCO levels in MIL-125 (left) and ICGM-1 (no NH_2; right).

Table 1. Effective Mass of Electron (m* electron) Computed at the Conduction Band Minima (CBM) in Electron Rest Mass Units m0 of the MIL-125 and ICGM-1 (no NH2) Computed Using the PBEsol Functional at Different k-Point Paths

MIL-125		ICGM-1 (no NH_2)	
K-PATH	m* electron, m_0	K-PATH	m* electron, m_0
Z → Γ	0.674	Γ → A	>50
Γ → X	>50	Γ → K	0.913
N → Γ	1.438	Γ → M	0.964